Journal of Thermal Science Vol.29, No.3 (2020) 772−783

https://doi.org/10.1007/s11630-020-1287-1 **Article ID: 1003-2169(2020)03-0772-12**

Experimental Investigation on the Adiabatic Film Effectiveness for Counter-Inclined Simple and Laid-Back Film-Holes of Leading Edge

YE Lin[1], LIU Cunliang[1,2*], XU Zhipeng[1], ZHU Huiren[1,2], LIU Haiyong[1,2], ZHAI Yingni[3,4*]

1. School of Power and Energy, Northwestern Polytechnical University, Xi'an 710072, China
2. Shaanxi Key Laboratory of Thermal Sciences in Aero-engine System, Xi'an 710129, China
3. State Key Laboratory of Green Building in Western China, Xi'an University of Architecture and Technology, Xi'an 710055, China
4. School of Mechanical & Electrical Engineering, Xi'an University of Architecture and Technology, Xi'an 710055, China

Abstract: The adiabatic film effectiveness η of the counter-inclined film-holes fed by varying internal coolant intake on the turbine vane leading edge model was experimentally investigated. A semi-cylinder model was adopted to model the vane leading edge which was arranged with two-row holes, which located at ±15° on both sides. The four Leading edge model with the combinations of hole-shape (simple holes and laid-back holes) and intake structure (plenum and impingement) were tested under four blowing ratios M of 0.5, 1.0, 1.5, and 2.0. The η contours were obtained by the transient measurement technique based on double thermochromic liquid-crystals. The results present that the η is sensitive to the M for the four studied leading edge cases. The addition of impingement enhances the η for the two studied holes. The film jets make the coolant-flow closed to the target surface, resulting in higher η under lower M. The core with higher η appears in the downstream area of hole-exit. The η enhancement can be provided to almost the identical level by adding the impingement-holes and improving the hole-exit shaping in most areas. With increasing M, the jets with stronger exit normal momentum penetrate into the main-flow. The impingement addition may be a more effective program to upgrade the η relatively to the exit shaping under larger M. Besides, the laid-back holes with impingement case produce the highest film cooling performance among the four cases, providing great potential in the leading edge especially under larger M.

Keywords: turbine blade leading edge, adiabatic film effectiveness, counter-inclined holes, impingement, thermochromic liquid crystal, transient measurement

1. Introduction

The ongoing effort to increase the gas turbine engine efficiency for power generation and aircraft propulsion has pushed the overall pressure ratio and corresponding turbine inlet temperature [1], which has been increasingly raised over the melting point of the turbine blade materials. Since the impact effect of hot gas, the leading edge (LE) experiences a strong thermal load. In the past decades, film cooling, by injecting the coolant flow bled

Received: Aug 02, 2019
AE: KAN Xiaoxu
Corresponding author: LIU Cunliang; ZHAI Yingni
E-mail: liucunliang@nwpu.edu.cn ynzhai2013@163.com

Nomenclature

D_f, D_i	diameter of semi-cylinder modeling leading edge and impingement tube/mm	T	temperature/K
d_f, d_i	diameter of film-hole and impingement hole/ mm	U	velocity/m/s
h	convective heat transfer coefficient/ W/m^2·K	X, Y, Z	coordinate of streamwise, normal to the model surface, and, spanwise/mm
M	blowing ratio	η	adiabatic film effectiveness
m, c	subscripts refer to the main-flow and secondary-flow	η_{la}	lateral-averaged adiabatic film effectiveness
Re	Reynolds number		

from the compressor into the blade passage through film-holes to form the insulating layer protecting the turbine blade surface [1, 2], has been one of the most critical cooling techniques. In addition, the impingement is also commonly adopted to improve the internal heat transfer for the LE [3, 4]. The present paper reports on an experimental investigation to aim at the internal coolant intake and hole-shape effects on the adiabatic film effectiveness η for the LE.

More recently, 90° compound angle holes with injection angle perpendicular to the main-flow direction are adopted on the LE. Han [1] and Bogard et al. [5] published overview about the heat transfer characteristics and cooling technologies in the LE cooling part. The cylindrical hole as the simple configuration is widely used on the LE cooling. A significant analysis and discussion using pressure-sensitive paint (PSP) method on the LE shape, density ratio ρ_c/ρ_m and blowing ratio M effect on LE cooling for simple holes were presented by Chowdhury et al. [6]. The data indicate that the gill film-holes are benefit to achieve improved coverage with high overall cooling effectiveness. Liu et al. [7] numerically investigated the LE film cooling of varying counter-inclined film-hole rows, and reported the corresponding mechanism on jet-interaction. The results demonstrated that the jet-interaction in the dual-row film cooling structure produces a more significant effect on the η than the heat transfer coefficient h. Li et al. [8] discussed the influence of wall-thickness variation on a full-coverage film cooled turbine blade in the stationary and linear cascade utilizing the PSP technique. The 6-row simple holes were drilled on the LE to construct showerhead film cooling. The results indicated that the wall thickness variation produces the marginal effect on the η for LE. Chen et al. [9] investigated the effect of unsteady wake on the LE film cooling with 3-row simple holes using the PSP technique. They found that the wake weakens the strength of the direct impingement of the main-flow on the LE, leading to a decrease in the film-coverage range. Additionally, a series of experimental investigations by Li et al. [10–12] were performed to study the effects of the rotation, injection angle, main-flow Reynolds numbers Re_m, ρ_c/ρ_m and M on the η distributions of the LE region of a twist turbine blade using a thermochromic liquid crystal (LC) technique. The LE cooling holes used in these studies are all the simple holes. Maikell et al. [13] further experimentally demonstrated the influence of the thermal barrier coating on overall cooling effectiveness for LE. The models with single row and 3-row simple holes were tested. The result indicates that the overall cooling effectiveness of the models with the thermal barrier coating increased for the interface between the base model and the coating, however it decreased on the external surface compared with the models with no coating.

Distinct improvements on film coverage are obtained by using the shaped holes, which have a diffusing expansion at the hole-exit [14]. A series of experimental investigations [15, 16] were compared for the η of simple holes and shaped holes, including the laid-back holes, fan-shaped holes, and teardrop-shaped holes, then the research confirmed that the holes with shaped-exit gave higher η than the simple hole, and the laid-back holes produced the highest η among the studied cases. Recently, there is a large volume of published studies describing the role of the shaped holes on the LE cooling. Similar hole shape setting was studied by Lu et al. [17] using transient infrared thermography technology, and consistent conclusions were obtained. Liu et al. [18] numerically described the improvement of LE η for a turbine guide vane by the fan-shaped holes. Experiments used the PSP technique of shaped hole with varying M and ρ_c/ρ_m made by Li et al. [19] confirming that the shaped hole with radial-angle provided higher η compared to the compound-angle. In addition, the ρ_c/ρ_m has a more significant impact on LE cooling for simple holes compared to the shaped holes. Liu et al. [20, 21] further compared the η of the simple holes and laid-back holes with varying radial angles and hole pitches on the

LE model with the 3-row holes.

From the foregoing, the literature referenced above obviously indicates that the laid-back holes have significant advantages on the film cooling performance of the LE region. Actually, the impingement cooling, as a common internal cooling method in turbine blade, is adopted to the LE cooling in conjunction with film cooling to improve the heat transfer coefficient augmentation on the internal LE surface and then reduce net heat flux. However, the above research had paid attention to the film cooling hole configuration, and lacked the investigation on how the internal impingement cooling structure affects the film cooling performance on the external surface.

So far, there has been limited discussion regarding the film cooling performance on the external LE surface combined with impingement cooling. The impingement addition is expected to change the flow structure in the local region near the film-holes, thereby causing the local η variation for the external surface. Therefore, the research of the internal cooling effect on the film cooling of the LE case is more indispensable, especially for the counter-inclined film-holes structure, which is an effective method to solve the manufacturing problem in the vicinity of the vane endwall. Consequently, the main objective of the present study is to experimentally report the potential improvement of film cooling of simple and laid-back film-holes with the counter-inclined type for varying intake structures of plenum and impingement by the transient LC measurement technique, and further explores the influences of impingement cooling on external η.

2. Experimental Setup

The schematic of an experimental system is illustrated in Fig. 1, and the detailed description of the facilities was given by Refs. [20, 21]. The independent centrifugal blowers provide the main-flow and the secondary-flow. The devices of main-path including the air tank with water-cooled device, valves, a settling chamber with rectifier and filter, two contraction sections, and mesh heater are used to ensure the uniform flow entering the test section. The width and height of test section are 220 mm and 120 mm, respectively. Three K-type OMEGA thermocouples measured the main-flow temperature T_m are inserted 50 mm upstream region of the LE model. By controlling the valve of main-path, the main-flow velocity U_m of the test section inlet, measured by the Pitot tube, is set at 15.4 m/s to ensure that the Re_m defined by U_m and semi-cylinder diameter D_f of the LE model is equal to 44 500. The turbulence intensity of the cross-section with the length of 140 mm along the upstream of the LE model measured by the hot-wire anemometer is 2%.

The secondary-flow flows in from the top inlet of the LE model as shown in Fig. 2. Three K-type OMEGA thermocouples are implanted in the test model cavity to obtain the secondary-flow temperature T_c. The ρ_c/ρ_m is nearly equal to 1.0 because of the relatively little temperature difference between main-flow and jet. By setting the MCR-Series Mass Gas Flow Controller for controlling the mass-flux of secondary-flow in the experiment process, then resulting in varying blowing ratios M, the M is expressed based on the U_m and averaged secondary-flow velocity at the hole-inlet which is calculated by averaging the total flow rate with the film-hole numbers and the cross-sectional area of the hole-inlet, and four values of 0.5, 1.0, 1.5, and 2.0 for M are tested in the present study. The test tunnel section is made of clear acrylic for optical access. A DV camera with light source is placed around the test tunnel, as indicated in Fig. 1, to record the color-changing process.

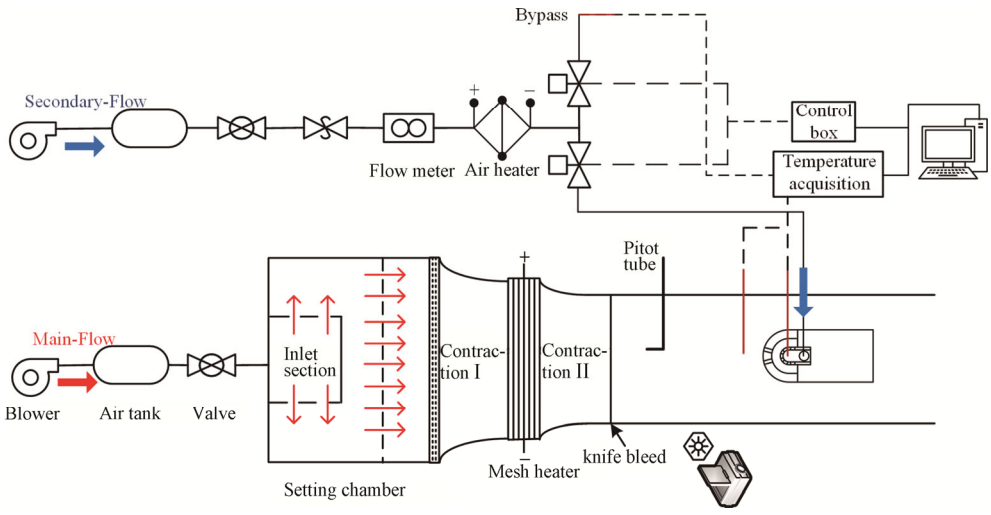

Fig. 1 Schematics of experimental setup used in the experiments

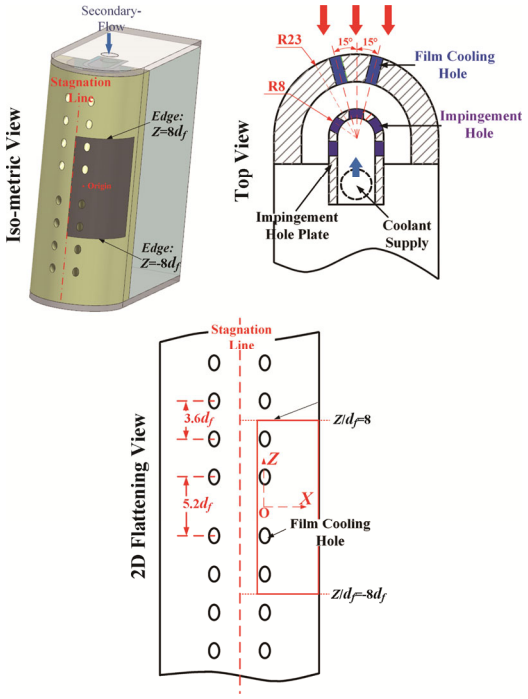

Fig. 2 Schematic view of leading edge model

The LE shape is simplified as a semi-cylinder model in the case of retaining key parameters, and the model is a combination of a semi-cylindrical body and an after blunt-body as presented in Fig. 2. Specifically, the outline of the original vane mid-section is adopted as the initial line of the leading edge model. The arc portion of the leading edge of the initial profile is approximately smoothed to a semi-circular arc. To ensure the same length-to-diameter ratio of the film-hole, the thickness of the semi-cylinder part of which the diameter D_f is 46 mm is controlled at 10 mm. The same simplified scheme is embodied by Chowdhury et al. [6] and Liu et al. [20, 21].

The η of simple holes and laid-back holes with the identical diameter and radial inclination angle are investigated and compared fed by different coolant channels in the present experiment. All the radially oriented film-holes have the identical cylinder part with the d_f of 3.2 mm, inclined to 45° with the spanwise direction and 90° with the flow direction. The laid-back holes have an additional forward expansion of 30° from the film-hole axis. The two rows of film-holes are arranged at the angular from the stagnation of 15° on both sides of the LE model and take aligned arrangement. The collinear counter-inclined film-hole row is designed for each row. Specifically, each row has the eight film-holes along the spanwise direction in the test surface, where the four holes at the top side incline to the $-Z$ side and the bottom four holes incline to the $+Z$ side, forming the counter-inclined structure. The hole-to- hole pitch between the two adjacent counter-inclined film-holes in the middle area is 5.2d_f in the spanwise direction, and the pitch between the two adjacent film-holes of the same direction is 3.6d_f.

As shown in Fig. 3, the four LE model with the combinations of hole-shape and intake structure, including the case of the simple holes fed by plenum without impingement (SH_P), the case of the simple holes with impingement (SH_I), the case of the laid-back holes fed by plenum without impingement (LBH_P), and the case of the laid-back holes with impingement (LBH_I), are considered in the present study. All the test models are made of Plexiglas with the density ρ of 1200 kg/m^3, the specific heat capacity c of 1470 J/(kg·K), and the thermal conductivity λ of 0.17 W/(m·K) tested by the Analytical & Testing Center of NPU. For the plenum cases of SH_P and LBH_P, the secondary-flow flows directly through the film-holes after entering the chamber. For the cases with impingement of SH_I and LBH_I, the secondary-flow passes through an arc-shaped impact plate with a diameter D_i of 16 mm and the wall thickness of 2.5 mm. All the impingement-hole (five-row of nine holes each) diameter d_i is 4 mm.

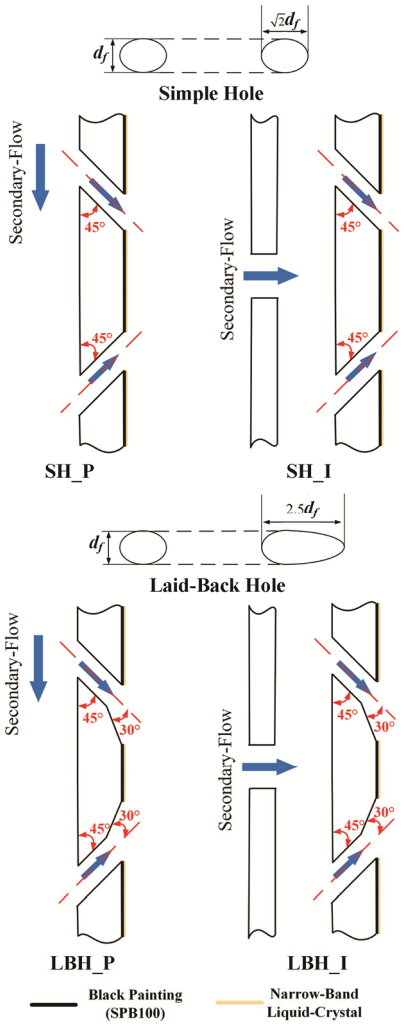

Fig. 3 Configurations of the studied film-holes

Fig. 2 gives a two-dimensional flattening schematic of the LE external surface. Due to the edge effect, the data in the present paper are based on the middle four film-holes per row. In addition, the contours are presented on the side of the cylinder due to the LE model symmetry. The region is marked with the gray block and the red dotted lines in Fig. 2. The main-low direction for this area is to the right.

3. Heat Transfer Measurement Approach

3.1 Transient measurement theory

The previous studies [20–22] reported detailed transient technique and narrow-band thermochromic LC, which are suitable for the present work. They also demonstrated the definite problem shown in Eq. (1) based on one-dimensional semi-infinite unsteady heat transfer.

$$T_s(t)-T_i=\left[1-\exp\left(\frac{h^2at}{\lambda^2}\right)erfc\left(\frac{h\sqrt{at}}{\lambda}\right)\right]\times\left[\eta T_c(t)+(1-\eta)T_m(t)-T_i\right] \tag{1}$$

The solution is the local surface temperature T_s(t) function with respect to time t. It is also the equation to calculate the two unknowns of the η and h. The film-cooling function for a semi-infinite flat plate has been given in previous studies. Since the LE configurations investigated in the present experiment is composed of a semi-cylinder body, the obtained heat transfer may be affected by the curvature effect. A simplified curvature effect model established by Buttsworth et al. [23], that the mathematic equation is given as Eq. (2), is applicable to the current cylindrical LE case if used within the limited measurement time.

$$T_s(t)-T_i=\frac{\sum_{n=0}^{N}A_n\eta\beta^{2n}X^{2n}}{1-\lambda/hD}+\frac{\sum_{m=0}^{N}B_m(1-\eta)\beta^{2m}Y^{2m}}{1-\lambda/hD}+\frac{T_i(E_0-1)}{1-\lambda/hD}$$

$$X^{2n}=\sum_{k=0}^{2n}\frac{\left(-\beta\sqrt{t}\right)^k}{\Gamma\left(\frac{k}{2}+1\right)}-E_0 \tag{2}$$

$$Y^{2m}=\sum_{k=0}^{2m}\frac{\left(-\beta\sqrt{t}\right)^k}{\Gamma\left(\frac{k}{2}+1\right)}-E_0$$

$$\beta=\frac{h-\lambda/D}{\sqrt{\rho c\lambda}}\qquad E_0=e^{\beta^2t}\cdot erfc\left(\beta\sqrt{t}\right)$$

The definition of the variables in Eqs. (1–2) can be found in Ref. [24].

According to Wagner et al. [25, 26], the approximate solution revealed in Eq. (2) takes curvature effects accurately into account as long as $\tau_R=4\lambda t/\rho cD^2<0.02$. For the test time, Schultz and Jones [27] provided a strict criterion for the maximum test time associated with thermal penetration distance δ of $t=\delta^2\rho c/16\lambda$. Then the time criterion from the assumption of a semi-infinite for the flat plate, $\tau_\delta=\lambda t/\rho c\delta^2<0.25$, is presented by Vogal and Weigand [28]. Wagner et al. [25] further verified that the time criterion from the flat wall investigation is also valid for a convex wall if the curvature effect is taken into account. In the present experiments, the time limits were respected.

For Eq. (2), 6 to 8 tests are carried out for the identical M in the traditional transient measurement, and multiple equations have been obtained to solve the inconsistent ensembles by using a least-squares regression procedure. In order to reduce the number of experiments, Vedula and Metzger [29] firstly introduced the double LC technique to measure the η of rows of inclined-holes. Then the double transient LC coating, the mixture of the two Hallcrest-made narrow-band LC, SPN/R25C1W and SPN/R30C1W, are applied to measure $T_s(t)$ distributions in the present work. A solution procedure that is equivalent to writing the equation for surface temperature twice, at each measurement location can then be adopted. Description of the double transient LC method can be referred to Ireland and Jones [30].

3.2 Liquid-crystal calibration

The transient LC calibration test is performed under the same light conditions as the experiments, taking into account the curved test surface and the angle between the camera and the light. In the calibration, the LE is replaced by a semi-cylindrical aluminum with the same external diameter and wall thickness as shown in Fig. 4. Its external surface is also painted with black painting and mixed transient LC coating. The color of the target surface gradually changes by heating the semi-cylindrical aluminum. The discoloration process is photographed and the temperature data are recorded synchronously.

Fig. 5 discusses the calibration curves of transient LC in the present study, including the correspondence between the green value intensity and local temperature of four different locations. The camera is stationary during the calibration process. The calibrations are run in the same light conditions with the experimental measurement, and the effects of lighting angle and view angle are also checked. Two peaks appear in the calibration data due to the double transient LC. It can be clearly seen that there exists obviously a difference in the green intensity peak at four locations. On the contrary, the corresponding temperatures extracted from Fig. 5 indicated in the block diagram are basically the same, in which the maximum differences on temperature are 0.04 K. Therefore, the

local green intensity peak is sought in the present transient process to determine the local T_s. The temperatures corresponding to the green intensity peaks are 299.88 K for R25C1W and 304.63 K for R30C1W, respectively.

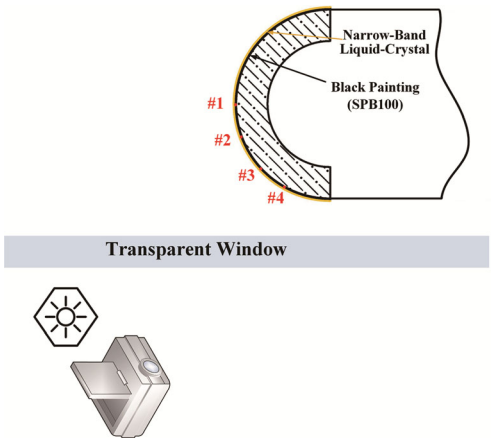

Fig. 4 Schematics of camera view and calibration

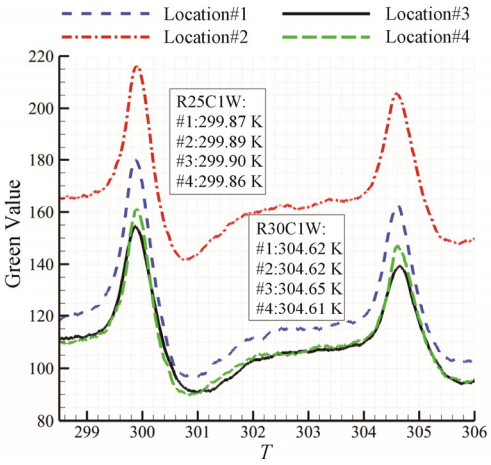

Fig. 5 The calibration curves of narrow-band LC

3.3 Measurement process and uncertainties analysis

Before starting a test, the T_m is stabilized at 296 K by adjusting the water-cooled valve. The LE model is blown for a sufficient period of time (≈1 hour) to obtain a uniform T_i. The heated secondary-flow discharged into the environment through a solenoid valve (see Fig. 1). The transient test is initiated by activating the solenoid valve of secondary-flow and the mesh heater of main-flow to introduce the heated main-flow and heated secondary-flow injection into the test section. Initiation of the test also triggers an automatic data acquisition system for recording thermocouple (T_m and T_c) readings in the main-flow and the secondary-flow. Different tests under an identical M are distinguished by varying the power of heating the main-flow and the secondary-flow to produce different $T_m(t)$ and $T_c(t)$.

Since there is a 4.75 K difference on the corresponding temperature of the two green value peaks in the present experiment, adjusting the T_m is adopted to prevent the LC of R25C1W changing color too fast or too slowly for R30C1W. Specifically, the voltage of the regulator that controls the mesh heater is set the low value to ensure that the temperature of heated main-flow is not too high (≈303 K), and then the heater voltage is rapidly increased so that the T_m rises to about 310 K after the LC of R25C1W completes the color change.

During the experiment, due to the non-uniformity on the flow direction and spanwise direction of the film cooling flow field and the temperature field, as well as the temperature gradient and lateral heat conduction inside the measuring plate, the inside of the measuring plate is not strictly one-dimensional heat conduction perpendicular to the wall direction. However, Vedula et al. [31] indicated the effect of the lateral heat conduction on the heat transfer results is limited of less than 3.5% in the transient heat transfer experiment where the heat transfer coefficient gradient is not very large.

The sequential perturbation method proposed by Moffat [32] is utilized to calculate the uncertainty of η, which mainly depends on the temperature, time and material property [33]. The estimated uncertainty intervals with a confidence interval of 95% for the present experiment are: $\Delta T_m=\Delta T_c=\Delta T_i=\Delta T_s=\pm 0.2$ K (ΔT_m and ΔT_c are measured by the K-type thermocouple. The uncertainty of thermocouple is ±0.2 K when measuring the temperature difference ΔT. Meanwhile, the LC calibration makes sure the T_s measured by LC have the same accuracy with the thermocouple.), $\Delta t=\pm 0.1$ s, $\Delta\sqrt{\rho c\lambda}=\pm 20$ J/m^2. Thus, the relative uncertainties on the local η are in the order of 20% for η=0.1 and 4% for η=0.7.

4. Results and Discussions

4.1 Adiabatic film effectiveness of simple holes

The η contours for the SH_P case and the SH_I case under lower M of 0.5/1.0 and larger M of 1.5/2.0 are presented in Fig. 6 and Fig. 7, respectively. The film jets make the coolant-flow close to the target surface, resulting in higher η to prevent the external surface from directly facing higher temperature main-flow. The shape of the hole-exit is filled in white to mark the relative position. The line at the central point of the hole-exit is defined as $X/d_f=0$. To evaluate the quality of film coverage numerically, the lateral-averaged adiabatic film effectiveness η_{la}, calculated from the relevant contours, is defined as the function of streamwise coordinate. The values of the η_{la} along the flow direction are calculated

from the corresponding contours and plotted in Fig. 8, where the hole-exit area of $-0.5 \leq X/d_f \leq 0.5$ is covered by gray block in the form of contour plots. Since 3-D heat conduction of the region around the hole-exit could lead to a remarkable uncertainty on the values, it is not considered for the quantitative discussion.

As indicated in Fig. 6(a), under M=0.5, a core area with higher η appears in the downstream area of hole-exit, and its distribution is slightly skewed to the inclination direction of the film-holes. For the SH_P case, the film coverage caused by the wall-ward flow due to small mass flow rate and momentum is concentrated. It results in almost no film coverage existing in the inter-hole region. Although the lateral spread of higher η increases due to the mixing of main-flow and coolant flow in the far-downstream region, the local η values in the range of $-1<Z/d_f<1$ are still below 0.15. As M increases to 1.0, the film jet covers larger area between the adjacent jets in the far-downstream area caused by larger jet flux; specifically, there exists no film-protection between the holes only in the range of $X/d_f<4$, and the lateral region is covered by the effective film with higher η as flowing downstream. As presented in Fig. 8, the η_{la} decreases first and then increases as the X/d_f increasing caused by the strongest normal momentum, which leads the film jets to lift off and then reattach. It is analogous in the result of the simple hole cases with 45° to the spanwise direction under M=1.0 in Ref. [20]. The η_{la} under M=1.0 is lower than that under M=0.5 by 12.9%–31.8% in the range of $X/d_f<4$, which mainly is due to the reduction of core high η. In the far-downstream area, there is no significant difference on the η_{la}. Compared with M=0.5 on the core higher η area, the core region has an angle-deviation along the lateral direction caused by lateral velocity component of the jet flow, which has been fully explained by Kim et al. [16] and Liu et al. [20].

For the SH_I case as illustrated in Fig. 6(b), with the addition of impingement under M=0.5, there is a

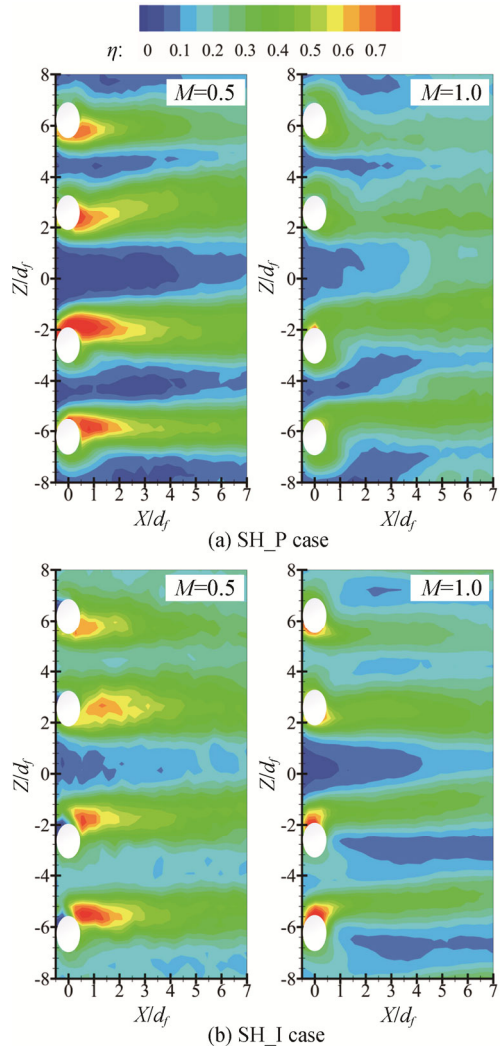

Fig. 6 η contours for simple holes under lower M

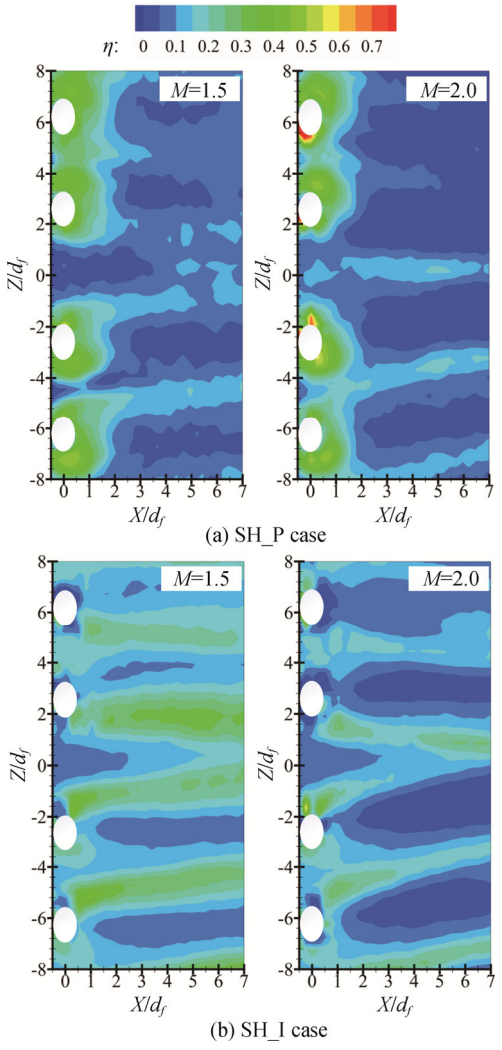

Fig. 7 η contours for simple holes under larger M

significant improvement on the η, especially for the lateral spread in the downstream region. Besides, the η in the area of the adjacent jets of the uniformly inclined-holes on both sides has a slight increase, whereas the film coverage in the region near the Z/d_f =0 still lists a disadvantage. As listed in Fig. 8, the η_{la} of the SH_I case is invariably higher than that of the SH_P case by 9.5%–30.1% under M=0.5, and the η decreases slowly along the flow direction. Under M=1.0, the η in the core region near the holes is relatively higher than that for the SH_P case. On the contrary, the η in the downstream area does decline, and the film coverage is more concentrated compared with the SH_P case. The above characteristics cause a convergence point on the η_{la} curves. Specifically, the SH_I has a slight advantage by a factor of 6.5%–13.4% in the upstream region of X/d_f<3.5, which is due to the improvement of the film coverage in the inter-hole area. Then in the downstream region, the disadvantage of the lateral spread on high η causes lower η_{la} to fall by 6.0%–16.2%. The dissimilar flow conditions at the hole-inlet produce varying velocity fields, thereby affecting the film cooling performance of the outer surface. Compared with the results in Fig. 6(a), it can be inferred that increasing the impingement hole to update the flow field is beneficial to the η of the simple hole in the LE region. The possible mechanism regarding the improvement is that the normal momentum of the jet core decreases with the additional impingement-holes the impingement-holes, leading to a reduction in the jet that is detached from the target surface and then blended with the main-flow. The η characteristic of each film-hole for the SH_I case is relatively consistent likely because of a more uniform flow distribution relative to the SH_P case.

The η of the LE model is also sensitive to the M. For increasing M to larger levels of 1.5 and 2.0, the jet is greater lifted off the target surface, which results in a detrimental influence on the η as indicated in Fig. 7. Compared with the results in Fig. 6, the peaks on the η value are lower and the regions of the film coverage are smaller for the identical case. For the SH_P case, the lift-off characteristic is more serious. The film is slightly covered in the downstream region, and almost no film coverage exists between the adjacent jets. On the contrary, the core region with higher η is obviously concentrated in the region near the film-holes of X/d_f<1.5. The distribution under two larger M is similar due to similar flow-field and velocity distribution, where the coverage of high η under M=1.5 is slightly larger. The SH_P case under M=1.5 produces higher η_{la} presented in Fig. 8, which exhibits 8.1%–59.4% higher value relative to M=2.0. For the SH_I case, the peak η value clearly appears in the downstream region. Although the film coverage is lower than that under lower M listed in Fig. 6(b), the wall-ward flow can still effectively extend to the downstream region, where the case under M=1.5 produces wider lateral extension and longer flow propagation. In the term of the η_{la} curves, there exist convergence points under a constant M due to the different peak η value locations. In the downstream region of X/d_f>2, higher η_{la} is displayed for the SH_I case, which exhibits 35.2%–152.3% and 20.6%–112.3% higher value relative to the SH_P case under M=1.5/2.0, respectively. Interestingly, the jets from the two adjacent counter-inclined holes in the middle region cross the centerline of Z/d_f=0 and then create a confluence, and this behavior was also reported by Liu et al. [7].

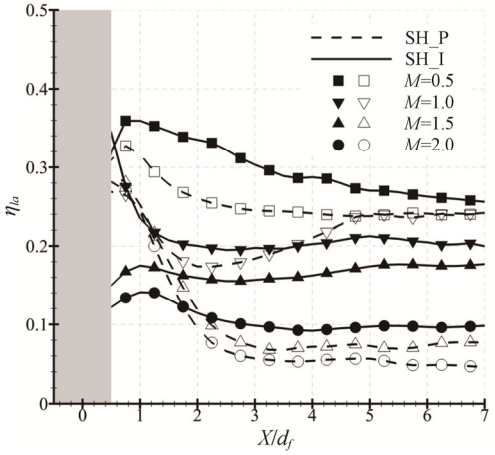

Fig. 8 η_{la} curves of simple holes under studied M

4.2 Adiabatic film effectiveness of laid-back holes

The η contours for the LBH_P case and the LBH_I case under lower M of 0.5/1.0 and larger M of 1.5/2.0 are presented in Fig. 9 and Fig. 10, respectively. Compared with the results for the SH_P case under lower M, the film jets of the laid-back holes provide higher η, and cover larger region especially for the cases under M=0.5. As discussed by Kim et al. [16], the spanwise-diffused hole significantly improves the η because of increasing lateral component and decreasing normal component on the jet momentum, resulting in a weakening of the penetration into the main-flow and the injecting to be more expansion into the spanwise direction. As presented in Fig. 9(a), in the upstream region near the film-holes, the area covered with high η is much larger. Compared to the peak η value, the LBH_P case has a relatively lower value than the SH_P case, whereas high η distribution is uniform in all studied region. With increasing M to 1.0, the η apparently decreases. The inter-hole area, X/d_f<1, can still maintain a more comprehensive coverage with high η, although there is no core covered with higher η like the contour under M=0.5. It leads to lower η_{la} under M=1.0 by a factor of 45.2%–48.4% as listed in Fig. 11. The film traces are weakened caused by slight lift-off of

film jets due to larger momentum in the region near the hole-exit, $1<X/d_f<4$, then reattach to the surface, and the area with high η is concentrated in the far-downstream region $X/d_f>4$. As demonstrated in Fig. 11, the η_{la} difference is reduced from 53.1% in the upstream $X/d_f=2$ to 19.6% in the far-downstream location of $X/d_f=6$. The benefit of adding impingement hole, the LBH_I case, is obviously illustrated in Fig. 9(b). Under $M=0.5$, the core higher η zone has a larger range, which is extended to $X/d_f=3$. There is a slight increase in the level of high η in the far-downstream region, which exhibits approximately 4.0% higher η_{la} relative to the LBH_P case under $M=0.5$ as presented in Fig. 11. The η_{la} decreases as jet flows downstream, and values tend to be uniform in the region $5<X/d_f<7$. The LBH_I case still maintains the advantage of the LBH_P case under $M=1.0$, and the range of low η is significantly reduced. Combined with the η_{la} development, the η_{la} falls sharply as the X/d_f increases in the upstream region of $X/d_f<2$. The significantly superior for the LBH_I case display in the range of $X/d_f<4$ compared with the LBH_P case under $M=1.0$. Continued downward development, it can be seen that the η_{la} value has been maintained around 0.23 for the LBH_I case, and there is no rebound trend like the LBH_P case.

As illustrated in Fig. 10, the lift-off characteristic is obvious for the studied cases of the laid-back holes as M increases to 1.5 and 2.0. It results in the conclusion that it is difficult to make the jet flow adhered to the target surface under larger M by limited structural and geometrical improvement discussed in this research. Obviously, the η for the case of the laid-back holes is improved by adding impingement-holes, which is also consistent with the simple hole case. In the term of the lateral-averaged value indicated in Fig. 11, in the range of $X/d_f<1.5$, the η_{la} difference is hard to compare between the two cases under two larger M. With increasing X/d_f, the difference for the LBH_P case is significantly expanded from 30.2% in the upstream X/d_f

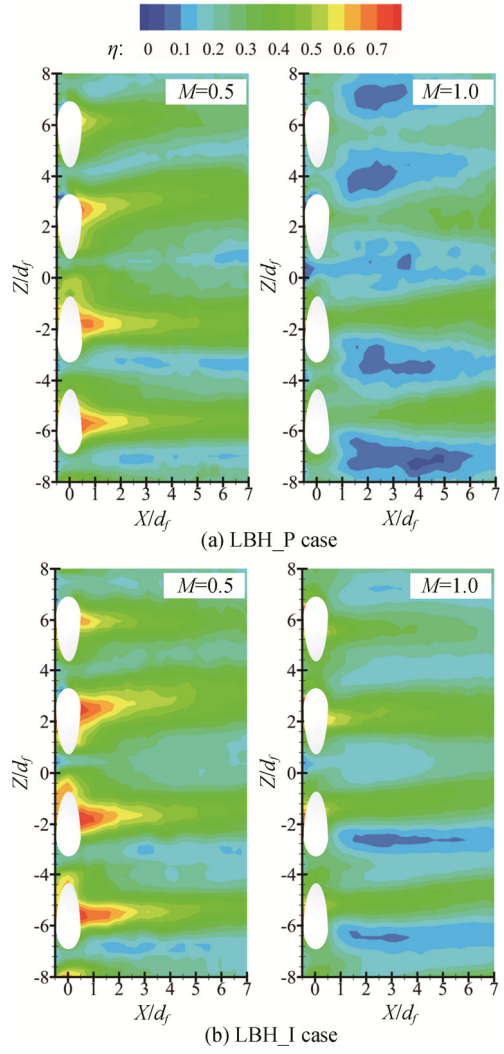

Fig. 9 η contours for laid-back holes under lower M

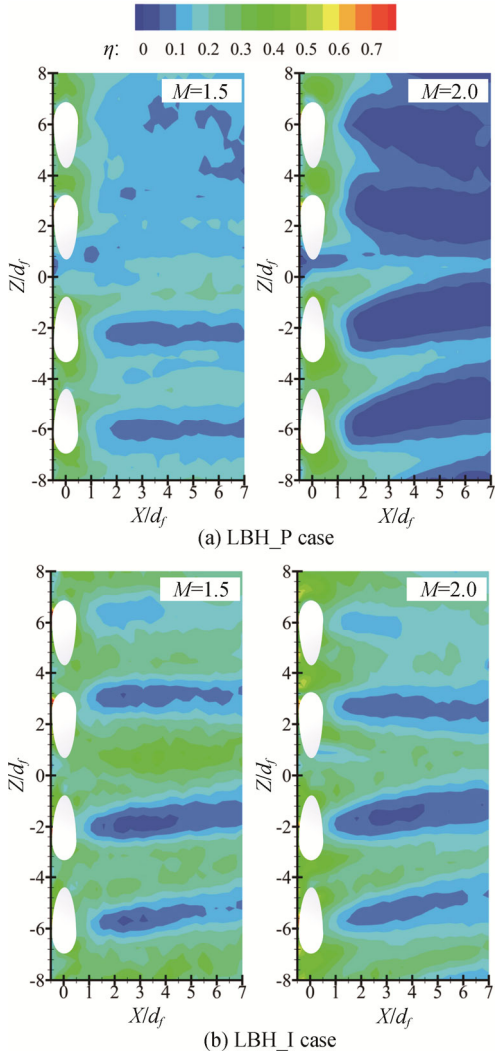

Fig. 10 η contours for laid-back holes under larger M

=2.5 to 57.4% in the far-downstream region of X/d_f=6.5. Combined with the contours listed in Fig. 10(a), the LBH_P case under M=1.0 has a large area that cannot be covered by the effective film-jets. On the contrary, the η_{la} difference for the LBH_I case under varying larger M has never been more than 17.9%. In the downstream region of X/d_f >2, lower η_{la} is presented for the LBH_P case, which exhibits 40.5%–51.6% and 66.7%–175.5% lower value relative to the LBH_I case under M=1.5/2.0, respectively.

Fig. 12 further illustrates the comparison of the η_{la} extracted from Fig. 8 and Fig. 11 for the four studied cases under lower M of 0.5 and larger M of 1.5, where solid line represents the measured experimental data of the case with impingement and the dotted line represents the case with plenum (without impingement). Overall,

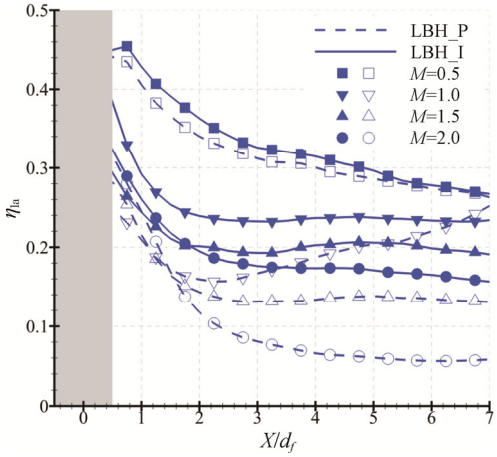

Fig. 11 η_{la} curves of laid-back holes under studied M.

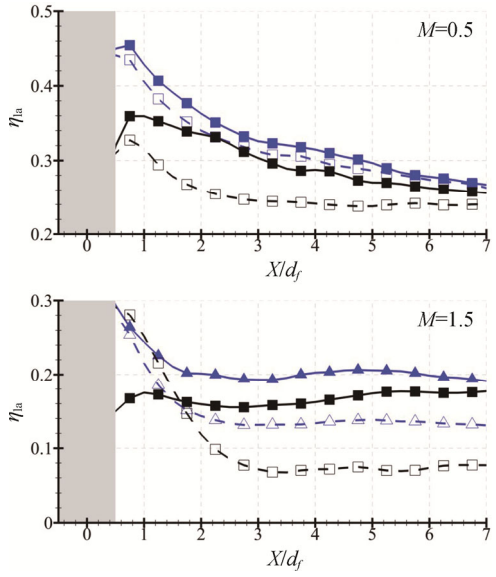

Fig. 12 Comparisons of the η_{la} for simple holes (black lines) and laid-back holes (blue lines).

the LBH_I case is the highest under a constant M, while the SH_P case is the lowest under a constant M in the downstream region of X/d_f >2. The η is at a relatively high level caused by small normal momentum and great film attachment under M=0.5. The η_{la} of the three cases except the SH_P case are approximately the identical level, especially in the downstream region. Among them, the LBH_I case has a slight advantage by a factor of 5.0%–9.9%. In the range of X/d_f <2, the η_{la} of the laid-back holes display the larger value than the simple holes caused by the η in the inter-hole area. Under M=1.5, the peak η_{la} value of each case has never been more than 0.3. The results clearly indicate the significant benefits of adding impingement-holes and improving hole-exit shaping. The SH_I case provides higher η_{la} than the LBH_P case in the most streamwise range. It presents that the impingement addition may be a more effective program to upgrade the η relatively to the exit shaping under larger M.

5. Conclusions

The adiabatic film effectiveness η of the counter-inclined film-holes fed by different intake structure on the LE model was experimentally investigated in the present paper. The transient LC measurement technique based on double thermochromic LC was employed to obtain the η contours for the four models with the combinations of hole-shape and intake structure. The main conclusions are as following:

(1) The η of the LE model is sensitive to the M for the four studied cases. The film jets make the coolant-flow close to the target surface, resulting in higher η under lower M. With increasing M, the jets with stronger exit normal momentum penetrate into the main-flow. The LBH_I case is the highest under a constant M, while the SH_P case is the lowest in the downstream region of X/d_f >2. The above results clearly indicate the significant benefits of adding impingement- holes and improving hole-exit shaping.

(2) At lower M, a core area with higher η appears in the downstream area of hole-exit. For the SH_P case, the film coverage caused by the wall-ward flow due to small mass flow rate and momentum is concentrated. It results in almost no film coverage existing in the inter-hole area. There is a significant improvement on the η with the impingement addition, especially for the lateral spread in the downstream region. The η in the area of the adjacent jets of the uniformly inclined-holes on both sides has a slight increase, whereas the film coverage in the region near Z/d_f=0 still lists a disadvantage.

(3) The film jets of the laid-back holes provide higher η for the cases of the laid-back hole, and cover larger region under lower M. Compared to the peak η value, the

LBH_P case has relatively lower value than the SH_P case, whereas high η distribution is uniform in all the studied ranges.

(4) The SH_I case provides higher η_{la} than the LBH_P case in most areas. The impingement addition may be a more effective program to upgrade the η under larger M.

Acknowledgment

The authors gratefully acknowledge the support of the National Natural Science Foundation of China (Grant No. 51776173), the Innovation Capacity Support Plan in Shaanxi Province of China (Grant No. 2019KJXX-065), the Scientific Research Plan Project of Key Laboratory of Shaanxi Provincial Education Department (Grant No. 17JS070), and the Innovation Foundation for Doctor Dissertation of Northwestern Polytechnical University (Grant No. CX201913).

References

[1] Han J.C., Dutta S., Ekkad S., Gas turbine heat transfer and cooling technology. CRC Press, Taylor & Francis, New York, 2012.

[2] Bogard D.G., Thole K.A., Gas turbine film cooling. Journal of Propulsion and Power, 2006, 22(2): 249–270.

[3] Zhou J., Wang X., Li, J., Li, Y., Effects of film cooling hole locations on flow and heat transfer characteristics of impingement/effusion cooling at turbine blade leading edge. International Journal of Heat and Mass Transfer, 2018, 126: 192–205.

[4] Zhou J., Wang X., Li, J., Influences of effusion hole diameter on impingement/effusion cooling performance at turbine blade leading edge. International Journal of Heat and Mass Transfer, 2019, 134: 1101–1118.

[5] Bogard D.G., Thole K.A., Gas turbine cooling. Journal of Propulsion Power, 2006, 22: 249–270.

[6] Chowdhury N.H.K., Qureshi S.A., Zhang M.J., Han J.C., Influence of turbine blade leading edge shape on film cooling with cylindrical holes. International Journal of Heat and Mass Transfer, 2017, 115(B): 895–908.

[7] Liu C.L., Zhao D., Zhai Y.N., Zhu H.R., He Y.H., Zhou Z.X., Investigations on the film cooling of counter-inclined film-hole row structures for turbine vane leading edge. International Journal of Turbo and Jet Engines, 2018, 35(3): 291–303.

[8] Li W.H., Li X.Y., Ren J., Jiang H.D., Experimental investigation of wall thickness and hole shape variation effects on full-coverage film cooling performance for a gas turbine vane. Applied Thermal Engineering, 2018, 144: 349–361.

[9] Chen D.W., Zhu H.R., Liu C.L., Li H.T., Li B.R., Zhou D.E., Combined effects of unsteady wake and free-stream turbulence on turbine blade film cooling with laid-back fan-shaped holes using PSP technique. International Journal of Heat and Mass Transfer, 2019, 133: 382–392.

[10] Li H.W., Han F., Zhou Z.Y., Ma Y.W., Tao Z., Experimental investigations of the effects of the injection angle and blowing ratio on the leading-edge film cooling of a rotating twisted turbine blade. International Journal of Heat and Mass Transfer, 2018, 127(B): 856–869.

[11] Li H.W., Han F., Wang H.C., Zhou Z.Y., Tao Z., Film cooling characteristics on the leading edge of a rotating turbine blade with various mainstream Reynolds numbers and coolant densities. International Journal of Heat and Mass Transfer, 2018, 127(B): 833–846.

[12] Li H.W., Han F., Ma Y.W., Wang H.C., Zhou Z.Y., Tao Z., Experimental investigation on the effects of rotation and the blowing ratio on the leading-edge film cooling of a twist turbine blade. International Journal of Heat and Mass Transfer, 2019, 129: 47–58.

[13] Maikell J., Bogard D.G., Piggush J., Kohli A., Experimental simulation of a film cooled turbine blade leading edge including thermal barrier coating effects. Journal of Turbomachinery, 2011, 133(1): 011014-011014-7.

[14] Bunker R.S., A review of shaped hole turbine film-cooling technology. Journal of Heat Transfer, 2005, 127: 441–453.

[15] Reiss H., Bölcs A., Experimental study of showerhead cooling on a cylinder comparing several configurations using cylindrical and shaped holes. Journal of Turbomachinery, 1999, 122(1): 161–169.

[16] Kim Y.J., Kim S.M., Influence of shaped injection holes on turbine blade leading edge film cooling. International Journal of Heat and Mass Transfer, 2004, 47(2): 245–256.

[17] Lu Y.P., Allison D., Ekkad S.V., Turbine blade showerhead film cooling: Influence of hole angle and shaping. International Journal of Heat and Fluid Flow, 2007, 28(5): 922–931.

[18] Liu J.J., An B.T., Liu J., Zhan W., Leading edge film cooling enhancement for an inlet guide vane with fan-shaped holes. Journal of Thermal Science, 2010, 19 (6): 514–518.

[19] Li S.J., Yang S.F., Han, J.C., Effect of coolant density on leading edge showerhead film cooling using the pressure sensitive paint measurement technique. Journal of Turbomachinery, 2013, 136 (5): 051011- 051011-10.

[20] Liu C.L., Zhu H.R., Zhang Z.W., Experimental investigation on the leading edge film cooling of cylindrical and laid-back holes with different hole pitches. International Journal of Heat and Mass Transfer, 2012, 55(23–24): 6832–6845.

[21] Liu C.L., Zhu H.R., Zhang X., Xu D.C., Zhang Z.W., Experimental investigation on the leading edge film cooling of cylindrical and laid-back holes with different

radial angles. International Journal of Heat and Mass Transfer, 2014, 71: 615–625.

[22] Ye L., Liu C.L., Zhu H.-R., Luo J.X., Experimental investigation on effect of cross-flow Reynolds number on adiabatic film effectiveness. AIAA Journal, 2019, 57(11): 4804–4818.

[23] Buttsworth D.R., Jones T.V., Radial conduction effects in transient heat transfer experiments. The Aeronautical Journal, 1997, 101(1005): 209–212.

[24] Ye L., Liu C.L., Liu F., Yang Y.Q., Zhu H.R., Experimental study on heat transfer of leading edge film-cooling with counter-inclined cylindrical and laid-back holes. ASME Journal of Heat Transfer, 2020. DOI: 10.1115/1.4046529.

[25] Wagner G., Kotulla M., Ott P., Weigand B., Wolfersdorf J. von, The transient liquid crystal technique: influence of surface curvature and finite wall thickness. Journal of Turbomachinery, 2005, 127(1): 175–182.

[26] Wagner G., Schneider E., Wolfersdorf J. von, Ott P., Weigand B., Method for analysis of showerhead film cooling experiments on highly curved surfaces. Experimental Thermal and Fluid Science, 2007, 31(4): 381–389.

[27] Schultz D.L., Jones T.V., Heat-transfer measurements in short-duration hypersonic facilities. Agardograph, 1973, 165: 155.

[28] Vogel G., Weigand B., A new evaluation method for transient liquid crystal experiments. 35th ASME National Heat Transfer Conference, Anaheim, CA, 2001, NHTC01-1511.

[29] Vedula R.J., Metzger D.E., A method for the simultaneous determination of local effectiveness and heat transfer distributions in three-temperature convection situations. ASME International Gas Turbine and Aeroengine Congress and Exposition, USA, Jun. 1991. 91-GT-345.

[30] Ireland P.T., Jones T.V., Liquid crystal measurements of heat transfer and surface shear stress. Measurement Science & Technology, 2000, 11(7): 969–986.

[31] Vedula R.P., Metzger D.E., Bickford W.B., Effects of lateral and anisotropic conduction on determination of local convection heat transfer characteristics with transient tests and surface coatings. ASME Journal of Heat Transfer, 1988, 104: 21–27.

[32] Moffat R.J., Describing the uncertainties in experimental results. Experimental Thermal and Fluid Science, 1988, 1(1): 3–17.

[33] Ye L., Liu C.L., Liu H.Y., Zhu H.R., Luo J.X., Experimental and numerical study on the effects of rib orientation angle on film cooling performance of compound angle holes. International Journal of Heat and Mass Transfer, 2018, 126: 1099–1112.